Ordu Üniv. Bil. Tek. Derg., Cilt:4, Sayı:2, 2014,70-82/Ordu Univ. J. Sci. Tech., Vol:4, No:2,2014,70-82

INVESTIGATION OF YOUNG'S MODULUS AND THERMAL EXPANSION COEFFICIENT EFFECTS ON TRANSIENT THERMAL ANALYSIS OF COATED TOOTH

Sadri Sen, Hamid Zamanlou*, Filiz Karabudak, Ruhi Yeşildal

Mechanical Engineering department, Engineering Faculty, Ataturk University, 25240-Erzurum, Turkey

*Corresponding author

ABSTRACT

Objective: to investigate the ideal combination of materials for tooth prosthesis.

Methods: Due to achieving fast results, the axisymmetrical finite element method (FEM) was used to compare stress distribution in a maxillary second premolar restored tooth by ANSYS program package. The five models (Model-1, Model-2, Model-3, Model-4, Model-5) were evaluated with different materials such as porcelain, Au-Pd, Ni-Cr, Ti, Zirconium. The tooth was assumed to be axisymmetric, non-directional features and elastic. Transient thermal stresses were studied in the models for different periods of time. Stress distribution of surfaces and interfaces were presented and they were evaluated with combine effect of Young's modulus and thermal expansion coefficient. The combine effects and their constituents were explicated by considering stress distribution and its point of effect.

Results: According to the results obtained by analyzing the numerical experiments; highest magnitude of stresses belongs to Model-4 which makes damage (separation and the formation of the interface crack) more likely to occur Model-5, Model-3, Model-1 and Model-2 follow Model-4 in a row.

Conclusion: Thermal expansion coefficient rate is the main reason of maximum stress distribution in first interface while rate of the elastic modulus causes the critical stress values in second interface with combination of Acrylic-NiCr-Cement-Dentin-Pulp-Alveoler bone in Model-4 and for this reason this model was chosen as the critical model. In comparison Model-4 with the other models, combination of Porcelain-Porcelain-Cement-Dentin-Pulp-Alveoler bone in Model-2 shows the better performance and recommended for clinical production modeling.

Keywords: Finite element method, dental coating, transient thermal stresses distribution

1.INTRODUCTION

Several types of materials and data have been settled for dental restorative crowns and dental prostheses. These materials must come across a number of mechanical, thermal principles in order to resist the inflexibilities of the submission. The most domineering of these properties are strength, fracture, compatibility with an oral environment, permeability and visual appearance. Similarly, the materials construction method should

be categorized by a good fit (i.e. dimensional accuracy), for this reason computer based methods and scientific analyses were established.

Toparli et al. show that during the imbibing of hot and cold liquids the temperature in the oral cavity go through rapid changes. However, the temperature of the dental tissues changes more slowly as the heat transfer to or from the teeth proceeds at a finite rate. The investigation effects of these thermal changes on restored teeth, and the associated bond failure and micro leakage, either in vitro or in vivo, present serious experimental difficulties. Mathematical modeling of the process using finite element analysis suggests an alternative approach of the problem, numerical study was carried out using three-dimensional finite element models and the tooth model was crowned with Au–Pd alloy, Ni–Cr alloy and porcelain. In the first part of the study, temperature changes as a result of hot/cold liquid in the mouth were considered [1].

A three-dimensional finite element analysis was completed [3]. All the nodes on the external surface of the root were constrained in all directions. Von Mises (equivalent stresses) energetic criterion was elected. In all the models the values of both strain and stress recorded at the middle third of the buccal aspect of the root surface were at their maxima. On the contrary, the minimum values were observed at level of both the apical portion of the post and the root apex. The maximum stresses were shown at level of the cemento–enamel junction (CEJ) on both the buccal and palatal aspects of root cement and dentin. Stress gradually decreased from the outer to the inner part of the root and from the CEJ towards the incisor margin of the crown as well.

To assess the effects of clinically relevant variables on the maximum principal stress (MPS) in the veneer layer of an anatomically correct veneer–core–cement–tooth model, MPS enlarged significantly with the addition of horizontal load components and with increasing cement thickness. In addition, MPS levels varied as a function of interactions between: proximal wall height reduction and load position; load position and cement thickness; core thickness and cement thickness; cement thickness and proximal wall height reduction; and core thickness, cement thickness and proximal wall height reduction [4].

The model of a multi-layer all-ceramic crown for posterior tooth 46 produced with CAD–CAM-technology was translated into a three-dimensional FEA program. This crown model was made with gold, zirconium, and alumina-based porcelain core and their matching veneering porcelains. The stress distribution due to the combined influences of bite forces, residual stresses instigated by the difference in expansion coefficient of the core material and the veneering porcelain, and the influence of shrinkage of the cement was investigated. Stiffer core material does not always for various reasons result in lower stresses in the veneering porcelain [5].

Dissemination and level of temperature, in a model of a maxillary canine was determined in the research [6]. The temperature distribution was determined by using a three-dimensional finite element analysis. The tooth was assumed to have undergone an endodontic treatment before the application. Heat applications of 200°C and 100°C

were considered. By using the virtual model and the simulation technique, the maximum temperature in the periodontal ligament was found to be 43.5°C.

Authorized finite-element (FE) model was used to perform the structural–thermal coupled field analyses and the Taguchi method was employed to identify the significance of each design factor in controlling the stress. The combined use of FE analysis and the Taguchi method efficiently identified that a deeper cavity might increase the risk of a restored tooth fracture, as well as a ceramic inlay with a lower thermal expansion, attaining a proper causal adjustment to reduce the lateral force and low modulus luting material application to obtain a better force transmission mechanism are recommended [7].

In this investigation, FEM is used to estimate thermal stress on the human second premolar coated tooth. That's why ANSYS package program is equipped to evaluate transient thermal stresses on mankind tooth. For this purpose by creating the five models each one including 6 regions, stresses dissemination are assessed according to thermal conditions. The objective of this study not only is to determine critical points in order to specify damage formations such as layers separation and crack increase, but also to utilize the optimum of the material combinations in dental prostheses models.

2.MATERIALS AND METHODS

This study was conducted by applying thermal load and calculation of transient stress analysis of human teeth. A coated tooth which has been damaged for any reason has been given geometrically in Fig. 1. Transient solutions continued until the pulp temperature reach to 45˚C, this specific temperature is maximum pulp viability temperature [8].

This model consists of six different regions, Region-1 (R1), Region-2 (R2), Region-3 (R3) that are required for the coating process, region-4 (R4), Region-5 (R5) and region-6 (R6) are prior to removal of the damaged regions. The coating thicknesses required for R1, R2, and R3 were 1.3, 0.5 and 0.3mm respectively. Due to the use of different material in the regions of R1 and R2, 5 (five) different models were prepared with dissimilar material properties, table. 2. Calculations carried out in elastic regions. By using the ANSYS package the models were created with rotational symmetry and half of any model was used to calculate two-dimensional analysis in the models (axisymmetric). In order to determine thermal stresses, two types of boundary condition are used in this paper: Structural (mechanical) boundary conditions and thermal boundary conditions [9].

Structural (mechanical) boundary conditions: As shown in fig. 2, all nodes between OA and AB are fixed. Y-axis is assumed rotational symmetry axis. It is assumed that, all the interfaces are integrated completely.

Thermal boundary conditions: In the model, the initial temperature, 36.5˚C, is considered as body temperature. While initial temperature is 36.5˚C, tooth surface temperature is defined as 50˚C. In the models prepared by different material properties (Model-1, Model-2, Model-3, Model-4, Model-5), thermal stress values are determined in upper surface, the first, second, third interfaces. From the calculation of cylindrical coordinates radial stresses $\sigma_{r,}$ tangential stresses $\sigma_{\Theta,}$ shear stresses $\tau_{r\Theta}$ and von Mises σ_{vm} plotted in diagrams.

Model-1 is created from 6 different regions that composed of various materials, as shown in Fig. 1. In this model upper surface modeled with porcelain, first interface

porcelain-zirconium, second surface zirconium-cement and third surface composed of cement - dentin.

Model-2, similarly made from 6 different regions as shown in Fig. 1, the material that respectively are used in this model for upper surface, first interface, second interface, third interface are : Porcelain, Porcelain-Porcelain, Porcelain-Cement, Cement-Dentin, table.1 and table. 2

Model-3, same as the Model.1 and Model.2, is composed of 6 sections in which upper surface including Acrylic, the first interface Acrylic-AuPd alloy, the second interface AuPd-cement and the third interface cement-dentin.

Model-4 is created from Acrylic on upper surface, Acrylic-NiCr on first interface, NiCr-Cement on second interface, Cement-Dentin for third interface.

Model-5, is composed of Acrylic on upper surface, Acrylic-Ti for first interface, Ti-Cement on second interface and Cement-Dentin for third interface.

Same routes of different models were plotted in graphics and σ_r, σ_Θ, $\tau_{r\Theta}$, σ_{vm} for each of them were analyzed.

To verify the results of the present model, the model created with data of reference 1 and 2. Results in comparison to them exposed a good agreement. Model of this study created with more elements and was well controlled, so this investigation exposed better results.

3.RESULTS

As shown in Fig 3.a. which denotes σ_r changes for upper surface in models, while significant changes occur in negative regions, Model-1 and Model-2, σ_r changes remain close to zero. Fig. 3.b, that states σ_r changes for first interface, σr changes in all of the models is close to the axis of symmetry (distance of 2mm), maximum positive and negative values is emerged in Model-3, Model-4, Model-5.

Fig. 3.c, shows the σr changes in second interface, all of the models fluctuations in negative and positive regions along the path. Likewise maximum values occur in Model-3, Model-4, Model-5. σr changes for third interface is exposed in Fig. 3.d. With the exception of model-2 changes take place along the lines in all models. While this change occur in negative regions for Model-1 in the others take place in positive regions dominantly. σr values reaches the greater values in the last part of this interface.

σ_Θ changes have been given respectively in Fig. 4.a-d. In upper surface for σ_Θ changes; Model-3, Model-4 and Model-5 in negative region have large fluctuations and the maximum values occur in Model-4. From Fig .4.b, for situation of first interface, Model-3, Model-4 and Model-5 have volatility in negative and positive region close to the axis of symmetry and maximum value for negative and positive region occurs in Model-4. Fig. 4.c, indicates σ_Θ changes in second interface, significant change for σ_Θ values happen in Model-3, Model-4 and Model-5, whereas Model-3 has the largest value, Model-4 and Model-5 are encountered in the near. Fig. 4.d. also include exchange curves of σ_Θ in the third interface, the largest value in negative region for Model-1 are remarkable.

$\tau_{r\Theta}$ changes during the lines are also available in Fig. 5.a-d. Significant change in upper surface along the line is shown in negative and positive region for Model-3, Model-4 and Model-5. Fig. 5.a. The values in these models are so closed to each other. Fig. 5.b. is given for changes in first surface. There are still noticeable change in Model-3,

Model-4 and Model-5. In spite of deviations in start and end point, the larger range of values is close to axis of symmetry. The maximum values occur in Model-4. From the Fig. 5.c, which is indicated $\tau_{r\Theta}$ changes for second interface, there are big fluctuation in the value of $\tau_{r\Theta}$ in Model-3, Model-4 and Model-5. Model-4 has the largest negative value and Model-3 and Model-5 reaching the close values of Model-4. Fig. 5.d, shows the status of $\tau_{r\Theta}$ in third interface.

σ_{vm} stresses are given in Fig. 6.a-d. Fig. 6.a, where the changes of upper surface is, shows that Model-3, Model-4 and Model-5 have the largest value which is close to axis of symmetry. The largest value is emerged in Model-4. Second interface has similar situation, this situation take place a little far away from the axis. Fig. 6.c. Third interface is slightly more complicated than the others, shown in Fig. 6.d. Here the change in Model-1 observed to occur much more dominant.

In all of the models changes in the last part of the line especially in geometric design of the third interface should be taken into account.

Under the same conditions Model-1 and Model-2 have lower stress values than Model-3, Model-4 and Model-5 are caused by differences between elastic modulus.

σ_{vm} stresses distribution for Model-4 is shown in Fig. 7, when this figure evaluates with Fig. 3.c, 4.c, 5.a, 5.c, 6.a, 6.b, 6.c, stress regions which are located on model will be understood better.

4.DISCUSSION

According to the results elastic modulus and thermal expansion coefficient of materials used in the models have influence on stress values, but the elastic modulus is more effective than thermal expansion coefficient. Rates of elastic modulus and thermal expansion coefficient of the material at two sides of interfaces are set in Fig. 8.a.b. The graphics describe stress dissemination in regions of the constituent materials which are shown in Fig 3-7. From the figures it can be declared that the rate of elastic modulus are more effective on the stress values at the second interface while the rate of thermal expansion coefficients are more effective on the stress values at the first interface, because, compared with other interfaces, second interface has higher elastic modulus rate. In addition, this rate is the highest value at Model-4. This condition explains the reasons both why Model-4 is critical model among the others and why the second interface has the greater stress values. The rate of thermal expansion in the first interface is more than the others also this expresses the first interface is one of the critical interfaces.

5.CONCLUSION

Geometry of model created by 3 constant, error-free and coated surfaces. In this condition stress distribution under thermal load is examined. The results obtained from computer models, based on experiments:

i) In Model-1 evaluation of σ_r, σ_Θ and $\tau_{r\Theta}$ stresses shows that in first and second interface separation and/or crack formation is most likely. For σ_{vm} this situation in second interface is more prevalent than other lines. Sudden negative and positive stress values increase in the end regions of lateral parts of the tooth indicates high damages possibility.

ii) σ_r, σ_Θ and $\tau_{r\Theta}$ in Model-2 have low values and make less sway.

iii) For Model-3 critical situation emerges in the first and second interface and regions are closed to axis of symmetry. Intensified stresses in this model, σ_{vm} curves clarify both crack and the possibility of separation.

iv) From the stress point of view in Model-4, significant changes were founded approximate to axis of symmetry. σ_{vm} stresses in the upper surface and the first interface should be taken into account in terms of damage. Fig. 7.

v) Model-5 like Model-4 presents a similar behavior. In this model stress intensity is high.

In the terms of stress variance in Model-4, possibility of damage formation (the separation of interfaces and cracks formation) is high. Model-5,Model-3,Model-1 and Model-2 shows a similar behavior.

Fig. 3.a-d, Fig. 4.a-d and Fig. 5.a-d, express same type of stresses along the same lines (upper surface, the first, second and third interfaces) for different models (Model-1, Model-2, Model-3, Model-4 and Model-5). Damages result from curves of σ_r shown in Fig 3.a-d may occur in first and second interface of Model-3, Model-4 and model-5.

From the σ_Θ curves (Fig 4.a-d) the possibility of damage in the first and second interfaces of Model-3, Model-4 and Model-5 is evident.

$\tau_{r\Theta}$ stresses (Fig 5.a-b) in upper surface and second interface of Model-3, Model-4 and Model-5 are important in terms of damage possibility.

As the result of these assessments, σ_{vm} curves (Fig 6.a-d) in Model-4, Model-5 and Model-3 and respectively in the first interface, upper surface, the second and third interfaces show damage possibility. Model-1 and Model-2 is seen to be more secure in these conditions.

Results indicate that differences between elastic modulus and thermal expansion coefficient of model's interface increase the stresses value and affect their distribution. Fig. 8.a,b.

Thermal expansion coefficient rate is the main reason of maximum stress distribution in first interface while rate of the elastic modulus causes the critical stress values in second interface with combination of Acrylic-NiCr-Cement-Dentin-Pulp-Alveoler bone in Model-4 and for this reason Model-4 was chosen as critical model. In comparison with other models, combination of Porcelain- Porcelain-Cement-Dentin-Pulp-Alveoler bone in Model-2 shows the better performance and recommended for clinical production modeling.

REFERENCES

[1] Toparli, M., H. Aykul, and S. Sasaki, Temperature and thermal stress analysis of a crowned maxillary second premolar tooth using three-dimensional finite element method. Journal of oral rehabilitation, 2003. 30(1): p. 99-105.

[2] Toparli, M. and S. Sasaki, Finite element analysis of the temperature and thermal stress in a postrestored tooth. Journal of oral rehabilitation, 2003. 30(9): p. 921-926.

[3] Sorrentino, R., et al., Three-dimensional finite element analysis of strain and stress distributions in endodontically treated maxillary central incisors restored with diferent post, core and crown materials. Dental Materials, 2007. 23(8): p. 983-993.

[4] Rafferty, B.T., et al., Design features of a three-dimensional molar crown and related maximum principal stress. A finite element model study. Dental Materials, 2010. 26(2): p. 156-163.

[5] De Jager, N., M. de Kler, and J.M. van der Zel, The influence of different core material on the FEA-determined stress distribution in dental crowns. Dental Materials, 2006. 22(3): p. 234-242.

[6] Er, Ö., S.D. Yaman, and M. Hasan, Finite element analysis of the effects of thermal obturation in maxillary canine teeth. Oral Surgery, Oral Medicine, Oral Pathology, Oral Radiology, and Endodontology, 2007. 104(2): p. 277-286.

[7] Lin, M., et al., A review of heat transfer in human tooth—experimental characterization and mathematical modeling. Dental Materials, 2010. 26(6): p. 501-513.

[8] Nammour, S., et al., Evaluation of dental pulp temperature rise during photo-activated decontamination (PAD) of caries: an in vitro study. Lasers in medical science, 2010. 25(5): p. 651-654.

[9] Lee, S.Y., et al., Thermo-debonding mechanisms in dentin bonding systems using finite element analysis. Biomaterials, 2001. 22(2): p. 113-123.

[10] Andreaus, U., M. Colloca, and D. Iacoviello, Coupling image processing and stress analysis for damage identification in a human premolar tooth. Computer methods and programs in biomedicine, 2010.

[11] Lin, C.L., Y.H. Chang, and Y.F. Lin, Combining structural–thermal coupled field FE analysis and the Taguchi method to evaluate the relative contributions of multi-factors in a premolar adhesive MOD restoration. Journal of dentistry, 2008. 36(8): p. 626-636.

[12] Linsuwanont, P., J. Palamara, and H. Messer, An investigation of thermal stimulation in intact teeth. Archives of oral biology, 2007. 52(3): p. 218-227.

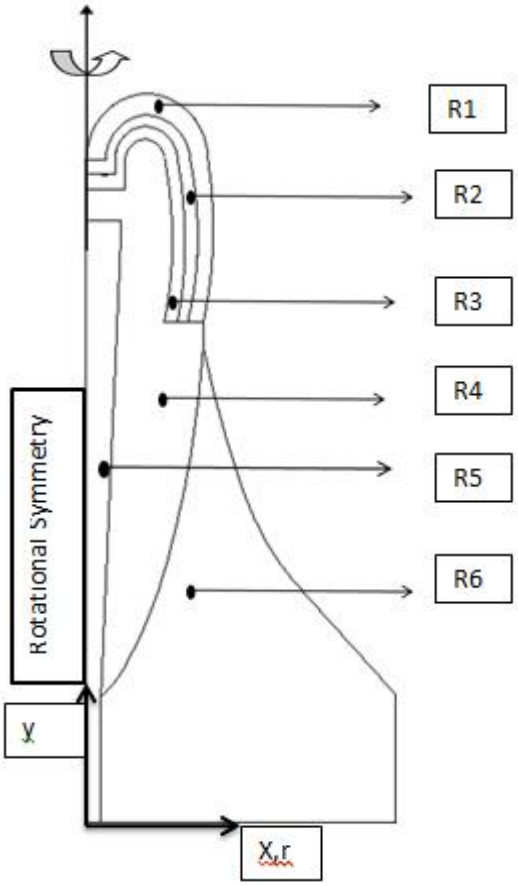

Fig. 1. View of the model used in the experiment

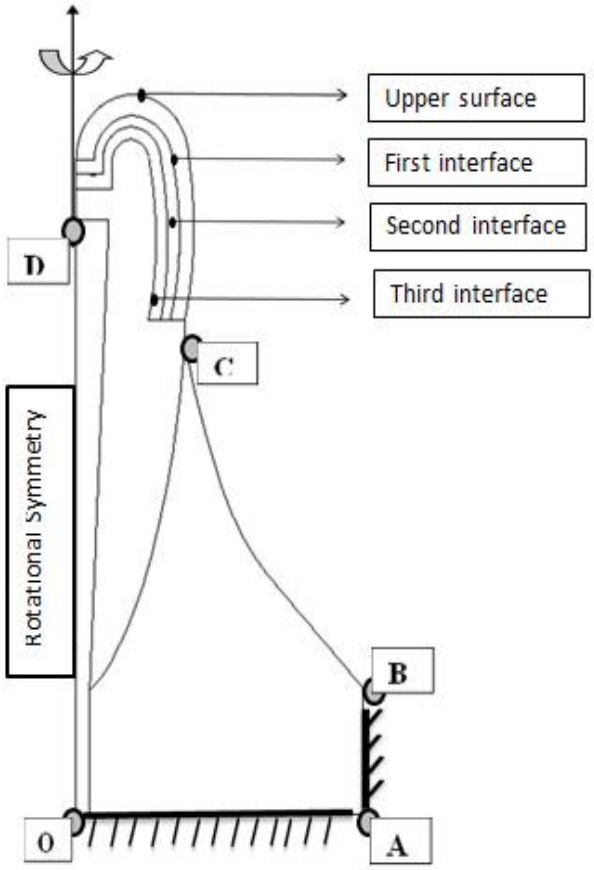

Fig. 2. Boundary condition and surfaces

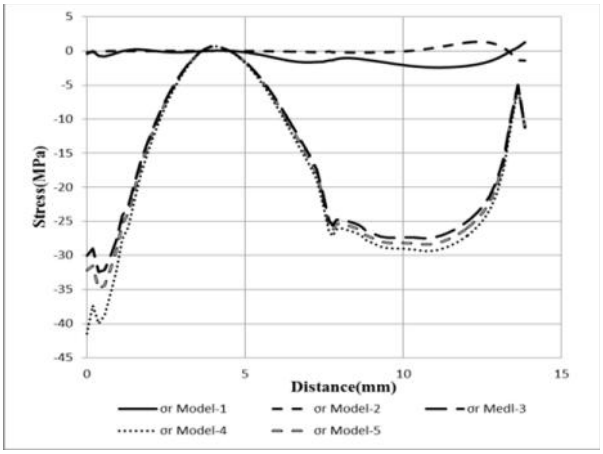

Fig. 3.a

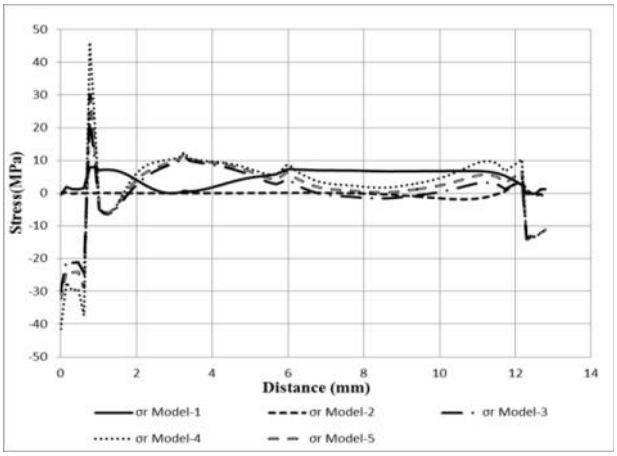

Fig .3.b

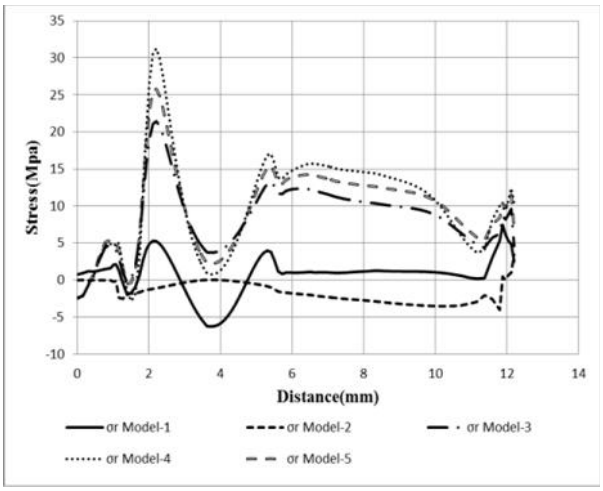

Fig. 3.c

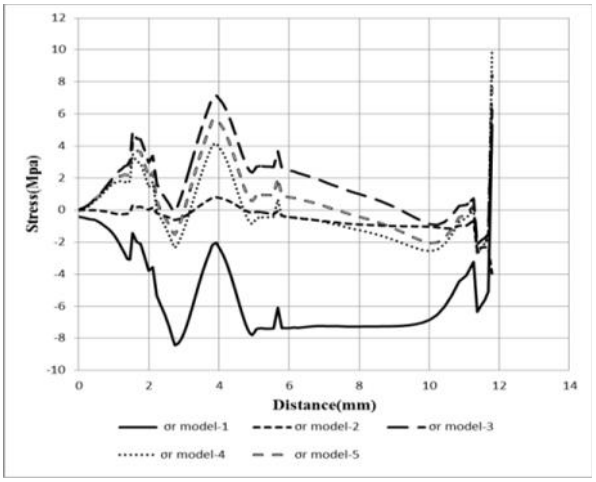

Fig. 3.d

Fig. 3. σr Stress curves for the same lines in different models: **a)** σ_r changes for upper surface in models, **b)** σ_r changes for first interface in models, **c)** σ_r changes for second interface in models, **d)** σ_r changes for third interface in models.

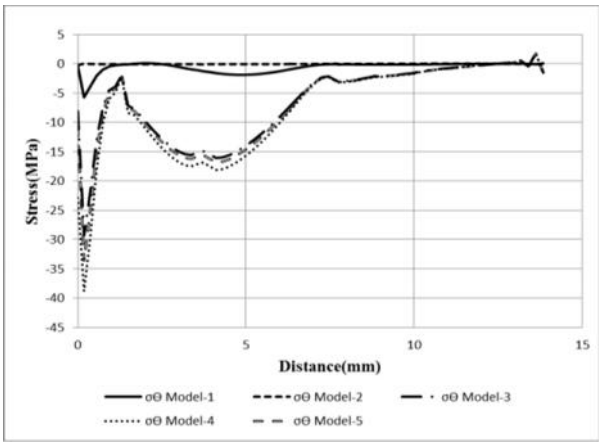

Fig. 4.a

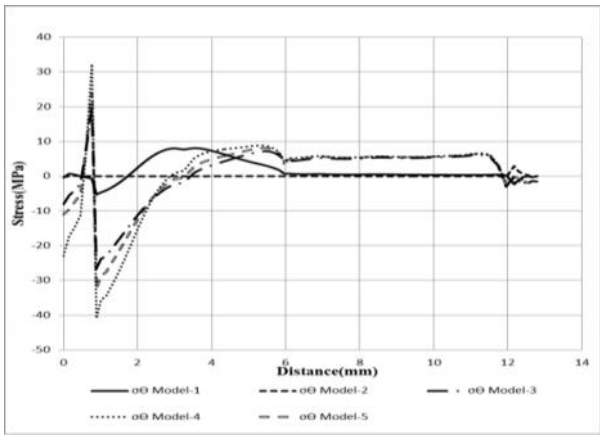

Fig. 4.b

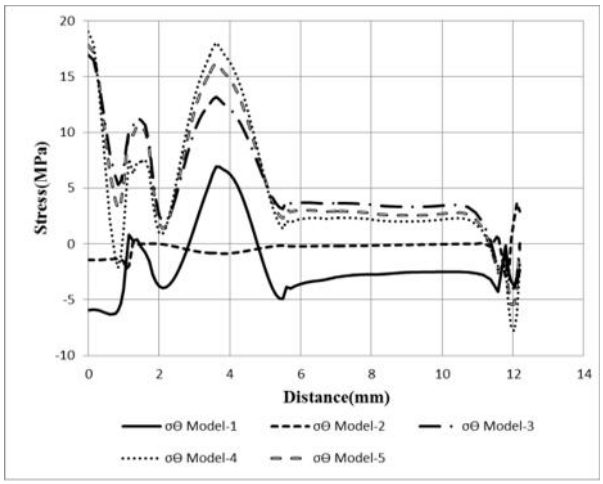

Fig. 4.c

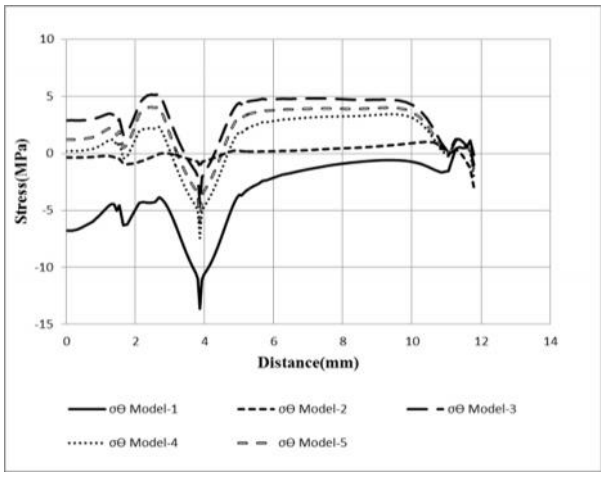

Fig. 4.d

Fig. 4. σ_Θ Stress curves for the same lines in different models; **a)** σ_Θ changes for upper surface in models, **b)** σ_Θ changes for first interface in models, **c)** σ_Θ changes for second interface in models, **d)** σ_Θ changes for third interface in models.

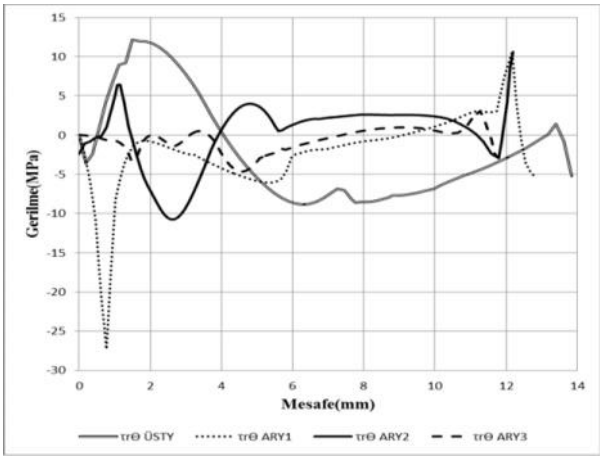

Fig. 5.a

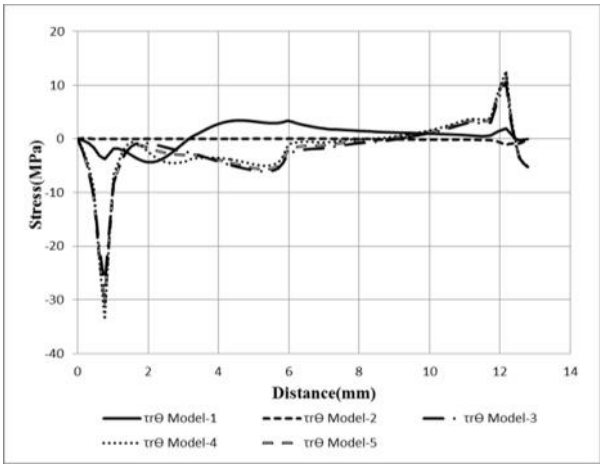

Fig. 5.b

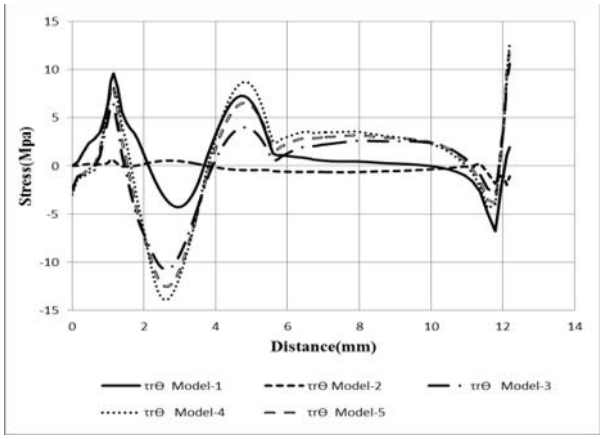

Fig. 5.c

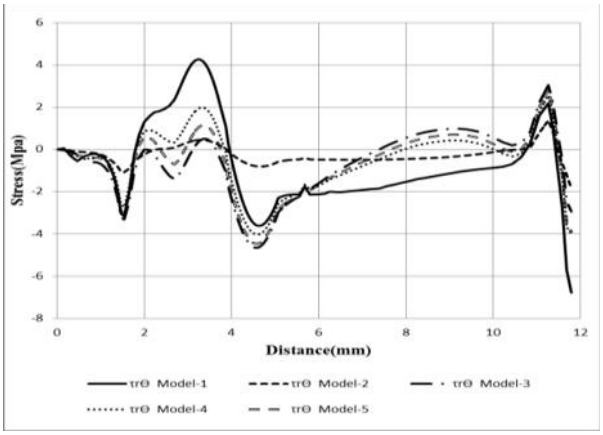

Fig. 5.d

Fig. 5. $\tau_{r\Theta}$ Stress curves for the same lines in different models**; a)** $\tau_{r\Theta}$ changes for upper surface in models, **b)** $\tau_{r\Theta}$ changes for first interface in models, **c)** $\tau_{r\Theta}$ changes for second interface in models, **d)** $\tau_{r\Theta}$ changes for third interface in models

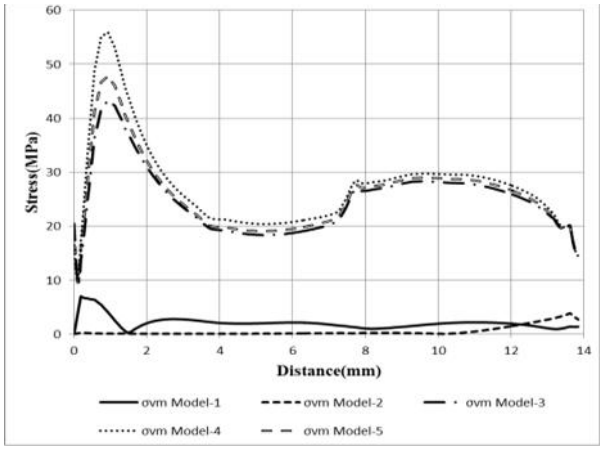

Fig. 6.a

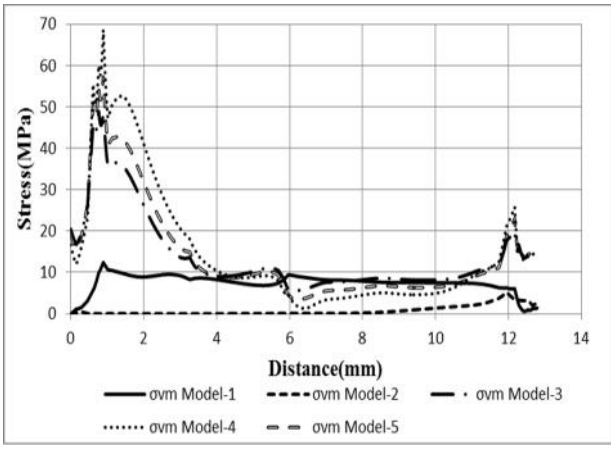

Fig. 6.b

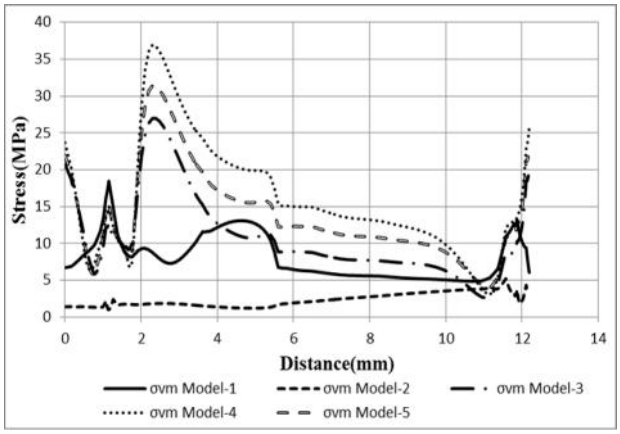

Fig. 6.c

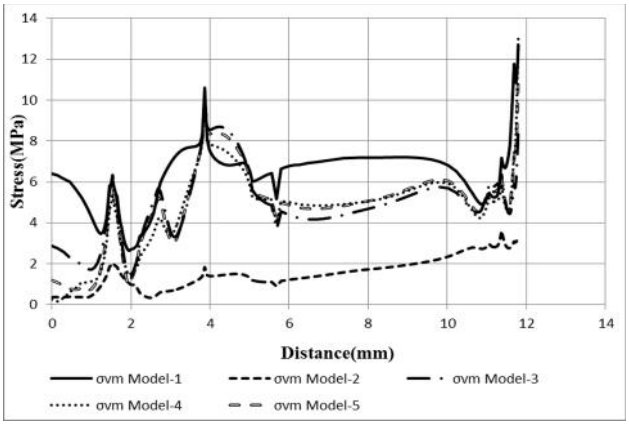

Fig. 6.d

Fig.6. σ_{vm} Stress curves for the same lines in different models; **a)** σ_{vm} changes for upper surface in models, **b)** σ_{vm} changes for first interface in models, **c)** σ_{vm} **c**hanges for second interface in models, **d)** σ_{vm} changes for thid interface in models.

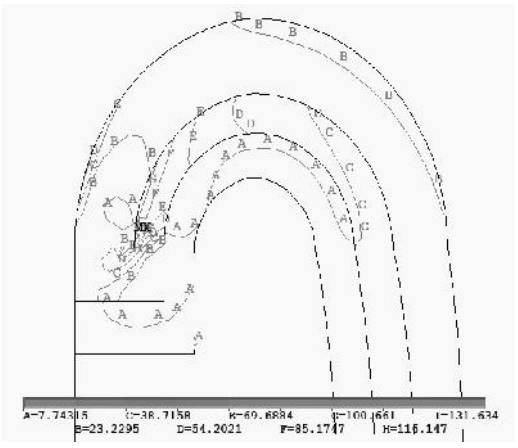

Fig. 7. σ_{vm} stresses in Model-4

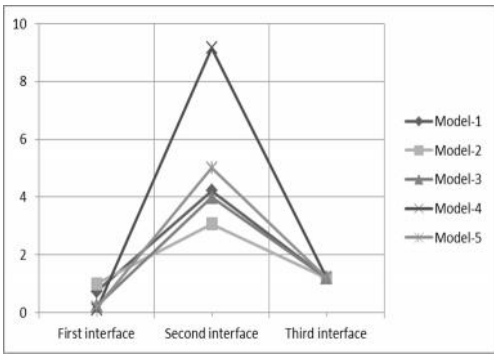

Fig. 8.a

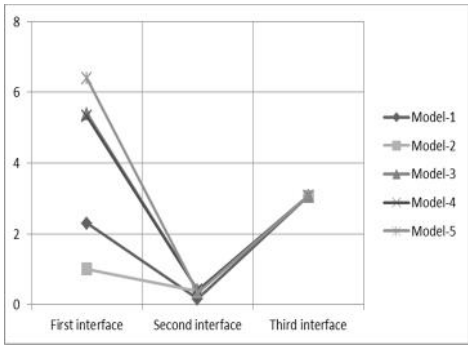

Fig. 8.b

Fig. 8. a) Rate of elastic modulus for interfaces, **b)** Rate of thermal expansion coefficient for interfaces

Table. 1. The materials that used in different regions of the 5 different models

Region / Model	R1	R2	R3	R4	R5	R6
Model-1	Porcelain	Zirconium	Cement	Dentin	Pulp	alveoler bone
Model-2	Porcelain	Porcelain	Cement	Dentin	Pulp	alveoler bone
Model-3	Acrylic	Au-Pd alloy	Cement	Dentin	Pulp	alveoler bone
Model-4	Acrylic	Ni-Cr alloy	Cement	Dentin	Pulp	alveoler bone
Model-5	Acrylic	Ti alloy	Cement	Dentin	Pulp	alveoler bone

Table. 2. Mechanical properties of materials used in the models

Properties / Materials	Modulus of elasticity (Mpa)	Poisson's ratio	Specific heat *(J/Kg˚C)*	Thermal expansion *(1/˚C)*	Thermal conductivity *(W/mm˚C)*	Density *(Kg/mm˚c)*
Zirconium	94500	0. 34	270	5.7E-6	2.3×10^-2	.0065×10^-3
Porcelain	68900	0.28	1070	13.1E-6	1.04×10^-3	.0024×10^-3
Au-Pd alloy	89500	0. 33	125	14.1E-6	1.2 ×10^-1	.00137×10^-3
Ni-Cr alloy	205000	0.33	450	14.3E-6	.92×10^-1	.0084×10^-3
Ti alloy	112000	0.33	544	11.9E-6	4.1×10^-3	.0045×10^-3
Acrylic	21100	0.35	1470	76E-6	1.9×10^-4	.0014×10^-3
Cement	22400	0.35	1250	35E-6	1.0467×10^-3	.0011×10^-3
Alveoler bone	13800	0.26	1260	10E-6	.5.86×10^-4	.0211×10^-3
Pulp	0.003	0.45	4200	180.1E-6	4.186×10^-2	.0010×10^-3
Dentin	18600	0.31	1600	11.4E-6	6.28×10^-4	.00196×10^-3